Polymorphism of even saturated carboxylic acids from *n*-decanoic to *n*-eicosanoic acid

Evelyn Moreno,[a] Raquel Cordobilla,[a] Teresa Calvet,*[a] M. A. Cuevas-Diarte,[a] Gabin Gbabode,[b] Philippe Negrier,[b] Denise Mondieig[b] and Harry A. J. Oonk[c]

Received (in Montpellier, France) 16th January 2007, Accepted 13th March 2007
First published as an Advance Article on the web 11th April 2007
DOI: 10.1039/b700551b

The polymorphism of normal saturated even carboxylic acids from *n*-decanoic to *n*-eicosanoic acid is discussed. Seven crystal modifications, including polymorphs and polytypes, were identified and fully characterized by the combination of calorimetric measurements (DSC) at atmospheric and high pressures, X-ray powder diffraction, FT-IR spectroscopy and scanning electron microscopy (SEM). All seven crystal forms, including polymorphs and polytypes, are observed at room temperature. Forms A_2 and A_{super} are triclinic, form C is monoclinic and forms E and B show both a monoclinic and an orthorhombic polytype. The triclinic modifications A_2 and A_{super} predominate for acids up to *n*-tetradecanoic acid ($C_{14}H_{27}O_2H$). The orthorhombic and the monoclinic forms predominate for acids from *n*-hexadecanoic ($C_{16}H_{31}O_2H$) up to *n*-eicosanoic acid ($C_{20}H_{39}O_2H$). When the temperature is increased, all the crystal modifications transform irreversibly to the C form. In the first part of this paper, cell parameters for the different forms are given, the observed temperatures and enthalpies of the transitions are reported and the stability of the different forms is discussed. In the second part, we state the main contribution of each technique for the identification and interpretation of the polymorphism of even numbered carboxylic acids.

Introduction

This work is the first part of a general study on the family of even saturated *n*-carboxylic acids undertaken within the REALM (Réseau Européen sur les Alliages Moléculaires) group, which works on the elaboration, structural and thermodynamic characterization, modeling, and applications of molecular alloy phase change materials (MAPCM) for energy storage and thermal protection. Previous studies of the *n*-alkane[1,2] and *n*-alkanol[3,4] families resulted in several commercialized industrial applications.[5–7] That encouraged us to undertake the study of the family of *n*-carboxylic acids, beginning with a polymorphism comprehension, since they are substances with high enthalpies of melting and, thus, promising candidates for the design of new MAPCMs.

The polymorphism of carboxylic acids has been discussed since the fifties but is still a matter of confusion and incompleteness due to the high number of crystalline forms that exist, the similarity of their structures, the difficulty of obtaining isolated forms, and the difficulty of growing single crystals of suitable quality for single crystal X-ray diffraction, which makes the identification and characterization of the different forms a difficult task. In this paper an account is given of our own systematic investigation on the polymorphism of the even saturated *n*-carboxylic acids, from decanoic to eicosanoic acid, by a complementary approach including X-ray powder diffraction, differential scanning calorimetry (DSC) at different pressures, Fourier transform infrared spectroscopy (FTIR) and scanning electron microscopy (SEM) techniques.

Normal saturated carboxylic acids with general formula $C_nH_{2n-1}O_2H$ exhibit a rich and complex polymorphic behaviour. The polymorphism of the acids depends on parity, and is a function of temperature. The appearance of a given form is influenced by the temperature and the rate of crystallization, the nature of the solvent, the purity of the acid itself and the number of carbon atoms in the chain.

A′, B′, C′, C″ and D′ crystal forms are mentioned for carboxylic acids with an odd number of carbon atoms and A_1, A_2, A_3, A_{super}, $B_{o/m}$, C and $E_{o/m}$ are mentioned for the even numbered ones.[8–11] In general terms, the packing of these forms consists of bilayers formed by dimers linked together through a typical $R_2^2(8)$ hydrogen bond pattern according to graph set notation.[12] A summary of the structural data reported in the literature is given in Table 1.

The structure of the C form[25,26] ($P2_1/a$, $Z = 4$) was determined from *in situ* crystallization and single crystal experiments. In this crystal form all the molecules in the asymmetric unit adopt an all-*trans* conformation. The dimers are arranged so as to exhibit terminal methyl and terminal carboxyl group monolayers parallel to the (0 0 1) plane (Fig. 1).

[a] *Departament de Cristallografia, Mineralogia i Dipósits Minerals, Facultat de Geologia, Universitat de Barcelona, C/ Martí i Franquès s/n, 08028 Barcelona, Spain. E-mail: mtcalvet@ub.edu; Fax: +34 93 402 1340; Tel: +34 93 402 1350*
[b] *Centre de Physique Moléculaire Optique et Hertzienne, UMR 5798 au CNRS Université Bordeaux I, Cours de la Libération 351, 33405 Talence Cedex, France*
[c] *Chemical Thermodynamics Group, Faculty of Chemistry, Utrecht University, Padualaan 8, NL-3584 CH Utrecht, The Netherlands*

Table 1 Bibliographic data for the carboxylic acid structures solved from single crystals

Phase	Acid	Space group	Z	Ref.
A_1	$C_{12}H_{23}O_2H$	Triclinic $P\bar{1}$	2	13
A_{super}	$C_{12}H_{23}O_2H$	Triclinic $P\bar{1}$	6	14
A′	$C_{13}H_{25}O_2H$	Triclinic $P\bar{1}$	2	15
A′	$C_{15}H_{29}O_2H$	Triclinic $P\bar{1}$	2	16, 17
B′	$C_{15}H_{29}O_2H$	Triclinic $P\bar{1}$	4	18
B′	$C_{17}H_{33}O_2H$	Triclinic $P\bar{1}$	4	19
B′	$C_{19}H_{37}O_2H$	Triclinic $P\bar{1}$	4	20
B_m	$C_{18}H_{35}O_2H$	Monoclinic $P2_1/a$	4	21
B_o	$C_{18}H_{35}O_2H$	Orthorhombic *Pbca*	8	22
E_m	$C_{18}H_{35}O_2H$	Monoclinic $P2_1/a$	4	23
E_o	$C_{18}H_{35}O_2H$	Orthorhombic *Pbca*	8	24
C	$C_6H_{11}O_2H$	Monoclinic $P2_1/a$	4	25[b]
C	$C_8H_{15}O_2H$	Monoclinic $P2_1/a$	4	25[b]
C	$C_{10}H_{19}O_2H$	Monoclinic $P2_1/a$	4	25[b]
C	$C_{12}H_{23}O_2H$	Monoclinic $P2_1/a$	4	25[b]
C	$C_{14}H_{27}O_2H$	Monoclinic $P2_1/a$	4	25[b]
C	$C_{16}H_{31}O_2H$	Monoclinic $P2_1/a$	4	26[b]
C	$C_{18}H_{35}O_2H$	Monoclinic $P2_1/a$	4	27[a]
C′	$C_7H_{13}O_2H$	Monoclinic $P2_1/a$	4	25[b]
C′	$C_9H_{17}O_2H$	Monoclinic $P2_1/a$	4	25[b]
C′	$C_{11}H_{21}O_2H$	Monoclinic $P2_1/a$	4	25[b]
C′	$C_{17}H_{33}O_2H$	Monoclinic $P2_1/a$	4	11
C′	$C_{19}H_{37}O_2H$	Monoclinic $P2_1/a$	4	11
C′	$C_{21}H_{41}O_2H$	Monoclinic $P2_1/a$	4	11
C′	$C_{23}H_{45}O_2H$	Monoclinic $P2_1/a$	4	11
C″	$C_{13}H_{25}O_2H$	Monoclinic $C2/c$	8	11, 25
C″	$C_{15}H_{29}O_2H$	Monoclinic $C2/c$	8	25, 11

[a] Structure solved from powder X-ray diffraction. [b] Structures originally reported in the conventional space group $P2_1/c$.

Crystals of the B and E forms observed for $C_{16}H_{31}O_2H$ and $C_{18}H_{35}O_2H$ are indistinguishable by means of their morphology. Structures of the B and E forms (Fig. 2) can be defined as conformational polymorphs: the molecules of the E form have an all-*trans* conformation whereas the molecules of the B form adopt a *gauche* conformation around the C_2–C_3 bond, as was determined from a spectroscopic study.[28] The difference in the molecular conformation does not affect significantly the position of the alkyl chains within the layers, the region between the methyl groups being identical in both forms. In addition, the B and E crystal forms of *n*-carboxylic acids exhibit polytypism, which arises from a different stacking sequence of the bilayers. A single bilayered monoclinic structure ($P2_1/a$, $Z = 4$), indicated with a subscript m, and a double bilayered orthorhombic structure (*Pbca*, $Z = 8$), indicated with a subscript o, were found for the B and the E forms of

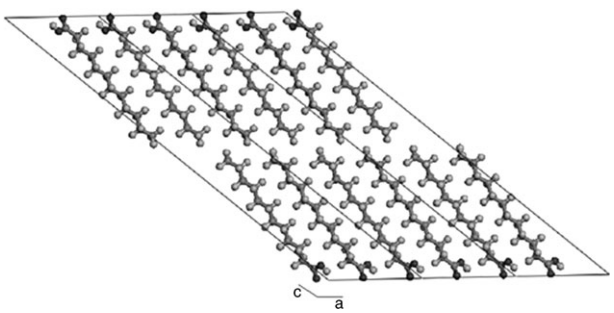

Fig. 1 Crystal packing showing three unit cells of the C form of $C_{12}H_{23}O_2H$[25] represented in the $P2_1/a$ space group.

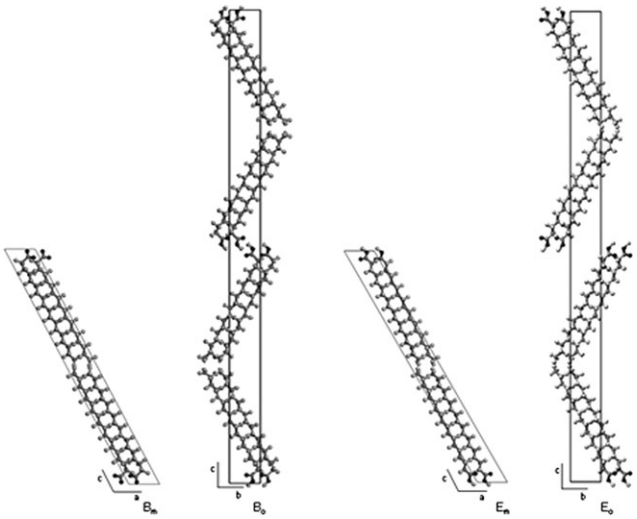

Fig. 2 Crystal packing of the B_m, B_o, E_m and E_o (left to right) forms of $C_{18}H_{35}O_2H$.[21–24]

$C_{18}H_{35}O_2H$.[21–24] As in the C form, the dimers of the B and E forms are arranged so as the methyl terminal groups and the carboxyl terminal groups gather in alternating monolayers.

Four different triclinic forms named A_1, A_2, A_3 and A_{super} are vaguely mentioned in the literature. The A_{super} form has space group $P\bar{1}$ with 6 molecules per unit cell.[14] However, von Sydow described the A_{super} form according to the usual description for long chain hydrogen bonded structures—in terms of the chain-packing of dimers—as $A\bar{1}$ space group, with 12 molecules per unit cell.[29] The 12 molecules are arranged such that, within a monolayer, three adjacent molecules have their carboxyl groups in one direction, and the next three molecules have their carboxyl groups in the opposite direction. There are two types of molecular conformation in the asymmetric unit. In one type, the hydrocarbon chain has an all-*trans* conformation (the plane of the carboxyl group is almost parallel to the plane of the hydrocarbon chain). In the other type, the carboxyl group is rotated along the C_1–C_2 bond (the plane of the carboxyl group is almost perpendicular to the plane of the hydrocarbon chain). In contrast with the A_{super} form, the A_1 form of $C_{12}H_{23}O_2H$ described by Lomer has $P\bar{1}$ space group and two molecules per unit cell.[13] The structure is such that, within a monolayer, the carboxyl group of one molecule is adjacent to the methyl group of the neighbouring molecule (Fig. 3). Thus, in the A_1 ($P\bar{1}$, $Z = 2$) and A_{super} ($A\bar{1}$, $Z = 12$) structures, a given terminal plane contains both methyl and carboxyl groups.

The form A_2 was first found by Kobayashi and co-workers, who carried out a spectroscopic study on acids $C_{14}H_{27}O_2H$ and $C_{16}H_{31}O_2H$.[30] They suggested a triclinic cell with separated carboxyl and methyl monolayers and with two types of molecules differing in the conformation of the carboxyl group. In their study they found that, when the temperature is decreased to 140 K, the A_2 form changes reversibly into the A_3 form. They observed a drastic change in the absorptions associated with the vibrations of the carboxyl group; possibly related to a rearrangement of the hydrogen bonds. To date the

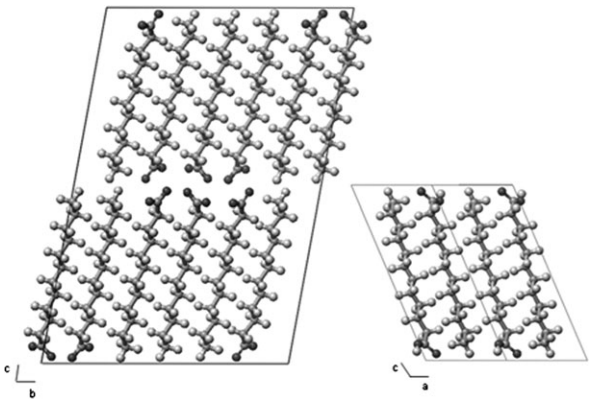

Fig. 3 Crystal packing of (left) the A_{super}[14] and (right) the A_1[13] (two cells represented) forms of $C_{12}H_{23}O_2H$.

structures of the A_2 and A_3 forms have not been solved from single crystal experiments.

Experimental

Materials

Samples of *n*-decanoic ($C_{10}H_{19}O_2H$), *n*-dodecanoic ($C_{12}H_{23}O_2H$), *n*-tetradecanoic ($C_{14}H_{27}O_2H$), *n*-hexadecanoic ($C_{16}H_{31}O_2H$), *n*-octadecanoic ($C_{18}H_{35}O_2H$) and *n*-eicosanoic ($C_{20}H_{39}O_2H$) acids were purchased from Fluka and Sigma. Their purity was $\geq 99\%$ according to GC-MS analyses. Experiments were performed on samples of the materials as purchased, on samples prepared by melting and quenching in liquid nitrogen, and on samples obtained from crystallization in pentane, isooctane, toluene, chloroform, ether and ethanol in a rapid and in a slow manner. Rapid crystallizations, yielding powder-like material, were carried out at room temperature, by passing a stream of nitrogen gas over a saturated solution. Slow crystallizations, giving larger crystals, were carried out at controlled constant temperature (298 K, 295 K, 283 K, 279 K, and 259 K) on saturated solutions, by evaporating the solvent in a gradual manner.

X-Ray powder diffraction analysis

Diffraction patterns were recorded in a horizontally-mounted, 120° and 25 cm of radius curved, position-sensitive detector INEL CPS-120 in transmission geometry. The detector was used in its 4096 channel resolution mode. Samples were placed in 0.5 mm diameter glass Lindemann capillaries. Cu K(α-1) radiation was selected by means of a Ge (1 1 1) primary flat monochromator. A parabolic multiplayer mirror, 'OSMIC Gutman optics # 13B-413', was placed between the tube and the monochromator. $Na_2Ca_3Al_2F_{14}$ (NAC) was used as an external standard to calibrate the detector and convert the channels to 2θ values. The data were linearized to a constant step size of 0.029° in 2θ by means of a cubic spline function. Calibration and linearization were performed with the Peakoc INEL software.[31] The acquisition times for the room temperature analysis were at least 13 h. The temperature dependent analyses were performed in the FURCAP device from INEL that enables heating of capillary samples from room temperature to 523 K. Data acquisition was carried out at several temperatures from room temperature to melting point, and such that, after 15 minutes of stabilization, diffraction patterns were recorded during 90 minutes.

Diffraction patterns of the C form were indexed using the X-Cell algorithm.[32] The final parameters of the C form were determined after Rietveld refinement of the structures solved by our group with MATERIALS STUDIO,[33,34] a software package for crystal structure determination from X-ray powder diffraction data. Diffraction patterns of the B and E forms were indexed using DICVOL[35] software and refined with the FULLPROF[36] program using the pattern matching option.

Infrared spectroscopy

The infrared spectra were obtained from a Bomem DA3 FTIR spectrometer equipped with a MCT (mercury–cadmium–telluride) detector. All samples were finely powdered and measured at room temperature using a diffuse reflection accessory (DRIFT) under a nitrogen gas atmosphere. The scanned range was 400–4000 cm^{-1}, with a resolution of 4 cm^{-1}. Each spectrum was recorded by averaging 100 scans.

Differential scanning calorimeter (DSC)

At atmospheric pressure, calorimetric measurements were made with a Perkin Elmer DSC-7 calorimeter. In sealed aluminium pans, the samples were heated, cooled and heated again, at a constant rate of 2 K min^{-1}. Analyses were performed from 273 K to reach the liquid phase. A minimum of three analyses per sample was done. The amount of sample used for each measurement ranged between 4.7 and 4.9 mg. The instrument was calibrated using indium and *n*-decane as external standards to determine temperature and enthalpy. The systematic uncertainties of temperatures and heat-flow calibration coefficients for the DSC were evaluated as ±0.2 K and ±2%, respectively. The random part of the uncertainties associated with each measurement was calculated according to the Student's method with a threshold of 95% reliability.

DTA measurements at different pressures were carried out with the equipment described by Pingel *et al.*[37] The samples were enclosed in small containers moulded from indium. Compressed silicon oil was used as a pressure medium and the temperature increase was adjusted to 2 K min^{-1}. The temperature values were measured with thermocouples during the heating run.

Scanning electron microscopy (SEM)

Images were taken to study the morphology of the different forms of the *n*-carboxylic acids. A Stereoscan 360 SEM (Cambridge Instruments Ltd), working at an accelerating voltage of 2 kV and a beam current of 60 to 70 pA, was used to observe the crystal shape of the $E_{m/o}$ forms. All samples were studied mounted on a biadhesive carbon sheet, and sputtered with gold. Due to the thermolability of the samples the sputtering was done at a very slow rate. A field emission SEM (model S-4100), working at an accelerating voltage of 5 kV and a beam current of 8 μA, was used to study the crystal shape of the $B_{m/o}$, C, A_2 and A_{super} forms. In this case the samples were sputtered with carbon.

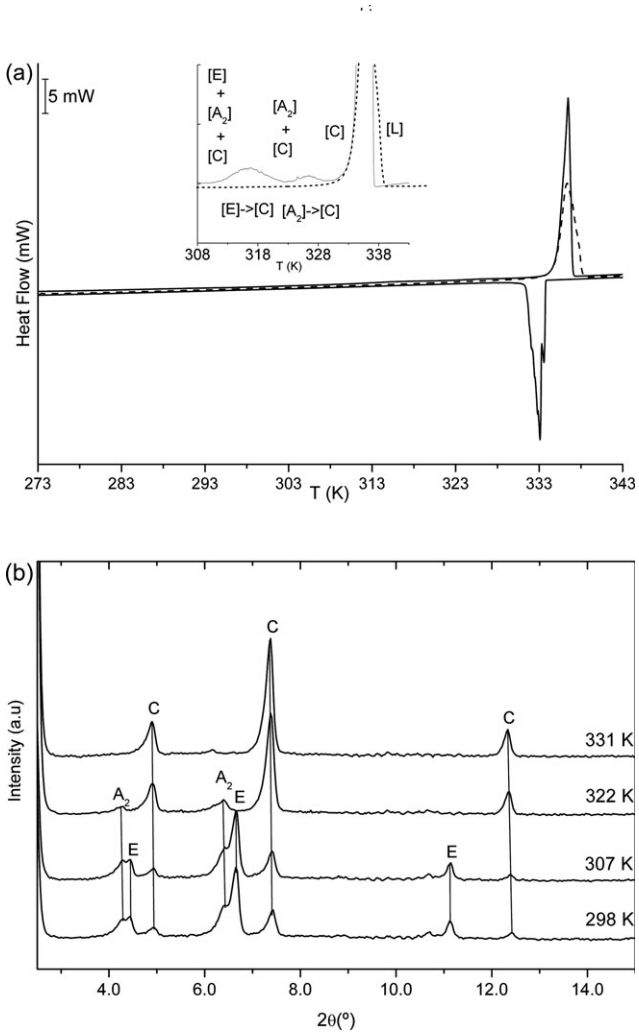

Fig. 4 (a) DSC analysis at 2 K min^{-1} and (b) powder X-ray diffraction patterns at increasing temperatures of a mixture of E, A_2 and C forms in a sample of $C_{16}H_{31}O_2H$. The inset in part (a) shows the first order solid–solid transitions from each individual form to the C form during the first heating process (solid line). Solid–solid transformations are not observed during the second heating process (dotted line).

Results and discussion

Occurrence of the different forms

Seven crystal forms called A_2, A_{super}, B_o, B_m, E_o, E_m and C, were observed in the present study for even *n*-carboxylic acids from ten to twenty carbon atoms. The different forms crystallize from solvents individually or, usually, as a mixture and do not convert to other forms at room temperature. On heating, all the forms transform irreversibly to the C form, before melting by means of a first order solid–solid transition, and recrystallize into the C form on cooling. On the second heating, only the melting of the C form is observed (Fig. 4). Thus, once the C form is obtained it remains stable.

The influence of the polarity of the solvent and the rate of crystallization on the polymorphism was studied systematically for $C_{14}H_{27}O_2H$ and $C_{16}H_{31}O_2H$, and to a lesser extent for the remaining acids. The results obtained are summarized in Table 2 and do not show any evidence of a systematic behaviour such as to control the "polymorphic purity" of the precipitate. The different crystal forms often crystallize together, yielding a mixture of polymorphs for all the acids studied. Nevertheless, some general tendencies regarding the occurrence of the different forms are observed.

Table 2 Crystal forms observed from room temperature crystallizations. Predominant forms are in bold and trace forms are between parentheses

	Rapid crystallization			Slow crystallization		
Acid	WPS[a]	IPS[b]	SPS[c]	WPS[a]	IPS[b]	SPS[c]
$C_{14}H_{27}O_2H$	**A_2** **A_{super}** C	**C** A_2 A_{super}	**C** (A_2)	**C**	**A_{super}** (C)	**C**
$C_{16}H_{31}O_2H$	**A_2** C $E_m(E_o)$	**E_m**(E_o) C	**C**	**C** A_2	**C** A_{super}	**B_m**
$C_{18}H_{35}O_2H$	**E_m** C	**E_m**(E_o)	—	**B_o** B_m **A_2**	**B_o** B_m **A_2** **E_m** **C**	—
$C_{20}H_{39}O_2H$	**E_m**	**E_m**(E_o)	—	**B_o**	**B_o** **E_m**	—

[a] WPS refers to weak polar solvents (pentane and isooctane). [b] IPS refers to intermediate polar solvents (toluene, chloroform and diethyl ether). [c] SPS refers to strong polar solvents (ethanol).

Acids $C_{10}H_{19}O_2H$ and $C_{12}H_{23}O_2H$ crystallize only as the C form in our study. However, other authors described the A_1 and the A_{super} forms for $C_{12}H_{23}O_2H$.[13,14] In addition, the occurrence of $C_{12}H_{23}O_2H$ in the B form was mentioned by Clark.[38]

Acid $C_{14}H_{27}O_2H$ crystallizes mainly as the triclinic A_2 and A_{super} forms for the majority of the rapid crystallization experiments, whereas the C form predominates for the slow crystallization experiments. Pure A_2 form is obtained from slow crystallization in pentane at 283 K. Pure A_{super} form is obtained from slow crystallization in diethyl ether at 298 K and pure C form is obtained from slow crystallization in isooctane at 295 K.

Acid $C_{16}H_{31}O_2H$ crystallizes as A_2, C and E_m, with traces of E_o form (denoted $E_m(E_o)$) from the rapid crystallization experiments. From slow crystallization experiments A_2, A_{super}, C and B_m forms are obtained. Independently of the crystallization rate, the A_2 form is obtained from weakly-polar solvents (pentane and isooctane). This form crystallizes as needle-like crystals in the walls of the crystallization vessel which are selected for their individual characterization. Pure A_{super} form is obtained from very slow crystallizations in toluene at 295 K. The B_m form is obtained from slow crystallization in ethanol at room temperature and in chloroform at 259 K. Pure C form is obtained in the vast majority of slow crystallization experiments at 298 K. Pure E_m form is never obtained as traces of E_o form are always present in the samples.

Acid $C_{18}H_{35}O_2H$ crystallizes as the E_m, with traces of E_o, and C forms from rapid crystallization experiments, the E_m form being the predominant one. Forms A_2, B_o, B_m, E_m and C are obtained from slow crystallizations, the B_o form being the predominant one. As for $C_{16}H_{31}O_2H$, crystals of the A_2 form

are selected for characterization from slow crystallizations in isooctane at 298 K. Pure B_m form was obtained from slow crystallization in toluene at 279 K. From toluene at 298 K, the B_o form with traces of B_m form was obtained.

Acid $C_{20}H_{39}O_2H$ crystallizes into the E_m and E_o forms from rapid crystallization experiments, the E_m form being the predominant one. From slow crystallization experiments the B_o and E_m forms were obtained the B_o being the predominant one. Pure B_o is obtained from slow crystallization experiments in toluene at 298 K. In addition, the B_m form, accompanied by traces of the B_o form, is obtained from slow crystallization experiments in toluene at 279 K.

Thermal behaviour and stability

The solid–solid transitions and the solid–liquid phenomena were analysed by means of DSC directly after the preparation of the sample (Table 3 and Table 4).

The literature data concerning the solid–solid transition are rather confused and incomplete; the polymorphs are not clearly specified and the data disagree among the different authors and with the results of the present investigation. The differences can be attributed to many factors: the purity of the samples, the nature of the solid phases involved and the method used to determine the transition temperatures.

Measurements of the solubility and the melting points of the B, C and A forms (without making any distinction between B_o and B_m and between the different A forms) were undertaken by Sato and co-workers[42] in order to determine their stability relationships. They measured the solubility of the B and C forms of $C_{18}H_{35}O_2H$ in *n*-decane, butanone and methanol at temperatures ranging from 271 to 311 K and found that B has the lowest solubility (is the most stable form) below 302 K, C having the lowest solubility above this temperature. Measurements carried out with the A form showed that it was metastable (higher solubilities) over the whole range of temperatures studied. Further experiments carried out by Sato point to the same conclusion: the B and C forms co-exist at certain temperatures (297, 305, 313 and 319 K for $C_{16}H_{31}O_2H$, $C_{18}H_{35}O_2H$, $C_{20}H_{39}O_2H$ and $C_{22}H_{43}O_2H$, respectively); B is stable below and C is stable above that temperature, A being metastable throughout.[9,43–45]

The differences regarding the temperature of the B → C transition between Sato's data (solubility measurements) and the present work (DSC measurements, Table 3) could be attributed to kinetic effects since the solid-state transitions between the polymorphic modifications are kinetically hindered due to certain steric effects involving rearrangements in the molecular conformation and the angle of tilt of the molecules within the cell.[9]

To confirm the stability regions determined by solubility experiments, DTA measurements at different pressures in the range 500–1500 bar were performed in order to determine the temperature–pressure equilibrium diagram.[46] Samples of $C_{18}H_{35}O_2H$ in C, B_o and E_m forms were used in the experiments, the B_o and E_m forms containing traces of B_m and E_o forms, respectively. The obtained results do not give any further information since the B_o → C and the E_m → C transitions cannot be detected with the equipment used. The

Table 3 Solid–solid transition measured temperatures and enthalpies

		Solid–solid transition[a]		
Acid	Phase	T/K	ΔH/kJ mol^{-1}	Ref.
$C_{12}H_{23}O_2H$	A_{super}	308.1		8
$C_{12}H_{23}O_2H$	B	283.1		38
$C_{14}H_{27}O_2H$	A_2	315.0 ± 1.5	1.8 ± 0.4	This work
$C_{14}H_{27}O_2H$	A_{super}	325.3 ± 0.4	6.4 ± 0.7	This work
$C_{14}H_{27}O_2H$	A	317.1		39
$C_{14}H_{27}O_2H$	B	298.1		38
$C_{16}H_{31}O_2H$	A_2	324.7 ± 0.6	2.6 ± 0.7	This work
$C_{16}H_{31}O_2H$	A_{super}	331.0 ± 0.5	7.6 ± 0.5	This work
$C_{16}H_{31}O_2H$	A	332.1		39
$C_{16}H_{31}O_2H$	E_m	316.7 ± 0.7	3.1 ± 0.2[c]	This work
$C_{16}H_{31}O_2H$	B_m	317.5 ± 0.6	4.9 ± 0.4	This work
$C_{16}H_{31}O_2H$	B	313.1		38
$C_{18}H_{35}O_2H$	A_2	331.6 ± 0.2	2.8 ± 0.3[b]	This work
$C_{18}H_{35}O_2H$	A	327.1		39
$C_{18}H_{35}O_2H$	A	337.1		9
$C_{18}H_{35}O_2H$	E_m	327.4 ± 0.6	4.3 ± 0.3[c]	This work
$C_{18}H_{35}O_2H$	E	316.6		9
$C_{18}H_{35}O_2H$	B_m	324.4 ± 0.7	5.4 ± 0.3	This work
$C_{18}H_{35}O_2H$	B_o	325.9 ± 0.5	5.7 ± 0.3[c]	This work
$C_{18}H_{35}O_2H$	B	324.1	5.1	9
$C_{18}H_{35}O_2H$	B	328.1		38
$C_{18}H_{35}O_2H$	B	319.1		39
$C_{20}H_{39}O_2H$	E_m	332.8 ± 0.4	4.1 ± 0.3	This work
$C_{20}H_{39}O_2H$	B_o	333.3 ± 0.6	6.1 ± 0.2	This work
$C_{20}H_{39}O_2H$	B_m	332.6 ± 0.4	5.9 ± 0.2[c]	This work
$C_{20}H_{39}O_2H$	B	325.1		39

[a] The solid–solid transition involves the transformation from the room temperature form to the C form. [b] Enthalpy obtained from one analysis. The error bar is estimated by comparison with the rest of the results. [c] The enthalpy is underestimated since traces of another form ($E_{o/m}$ or $B_{o/m}$) are present in the samples analyzed.

Table 4 Melting temperatures and enthalpies measured on heating at normal pressure. The solid–liquid transition always involves the transformation from the C form to liquid phase

Acid	T/K	ΔH/kJ mol^{-1}	Ref.
$C_{10}H_{19}O_2H$	303.8 ± 0.6	28.3 ± 0.7	This work
$C_{10}H_{19}O_2H$	305		25
$C_{10}H_{19}O_2H$	304.5 ± 0.1	28.0 ± 0.1	40
$C_{10}H_{19}O_2H$	304.7 ± 0.1	29.4 ± 1.2	41
$C_{12}H_{23}O_2H$	316.2 ± 0.4	36.1 ± 0.8	This work
$C_{12}H_{23}O_2H$	318		25
$C_{12}H_{23}O_2H$	317.1		39
$C_{12}H_{23}O_2H$	316.9 ± 0.1	36.3 ± 0.1	40
$C_{12}H_{23}O_2H$	317.2 ± 0.1	36.7 ± 1.5	41
$C_{14}H_{27}O_2H$	326.5 ± 0.5	45.0 ± 1.3	This work
$C_{14}H_{27}O_2H$	328		25
$C_{14}H_{27}O_2H$	327.3		39
$C_{14}H_{27}O_2H$	327.3 ± 0.1	45.1 ± 0.1	40
$C_{14}H_{27}O_2H$	327.4 ± 0.1	44.7 ± 1.8	41
$C_{16}H_{31}O_2H$	334.7 ± 0.5	53.0 ± 1.0	This work
$C_{16}H_{31}O_2H$	336.0		39
$C_{16}H_{31}O_2H$	335.6 ± 0.1	53.7 ± 0.1	40
$C_{16}H_{31}O_2H$	335.8 ± 0.1	53.4 ± 2.1	41
$C_{18}H_{35}O_2H$	342.4 ± 0.3	63.2 ± 1.4	This work
$C_{18}H_{35}O_2H$	342.8		39
$C_{18}H_{35}O_2H$	342.5 ± 0.1	61.2 ± 0.2	40
$C_{18}H_{35}O_2H$	342.6 ± 0.1	63.0 ± 2.5	41
$C_{20}H_{39}O_2H$	347.6 ± 0.3	71.6 ± 1.6	This work
$C_{20}H_{39}O_2H$	348.2		39
$C_{20}H_{39}O_2H$	348.2 ± 0.1	69.2 ± 0.4	40
$C_{20}H_{39}O_2H$	348.4 ± 0.1	72.0 ± 2.8	41

Table 5 Calculated lattice energies ($E_{lattice}$) of the C, E_o, E_m and B_o forms of $C_{18}H_{35}O_2H$ using the COMPASS force-field[47]

Crystal form	$\lvert E_{lattice}\rvert$/kJ mol^{-1}
C	189
E_o	194
E_m	194
B_o	195

energy of these transitions is not sufficiently large and the peaks not sufficiently sharp to give a reliable DTA signal. Only the melting phenomenon, which involves the transition from the C phase to liquid, is sufficiently energetic and sharp as to give a reliable signal.

To complement these results, lattice energy calculations were undertaken with the single crystal structures of the B_o,[22] E_m,[23] and E_o[24] forms of $C_{18}H_{35}O_2H$ available in the literature, and the structure of the C form solved from powder data in our group. Using the COMPASS[47] force-field, all the structures were fully optimized and the lattice energy calculated in order to predict the relative stability of the different polymorphs. The B_m form was discarded since the reported structure is incomplete; coordinates of the hydroxylic hydrogen are omitted. The enthalpy of sublimation, ΔH_{sub}, of a solid is the experimental thermodynamic quantity describing the stability of the crystal structure. This enthalpy can be defined by eqn (1), where the lattice energy, $E_{lattice}$, then constitutes an approximation to ΔH_{sub} and consequently to the stability of a crystal.[48] According to the calculated lattice energies displayed in Table 5, the B_o and the $E_{o/m}$ forms of $C_{18}H_{35}O_2H$ are more stable than the C form by 6 and 5 kJ mol^{-1}, respectively, at 0 K, which agrees with the conclusions reported by Sato from solubility experiments.

$$\Delta H_{sub} = -E_{lattice} - 2RT \quad (1)$$

Structural characterization

X-Ray measurements made with the INEL CPS 120 at room temperature were used for the crystallographic characterization. Cell parameters obtained after Rietveld refinement of the C form for acids from $C_{10}H_{19}O_2H$ up to $C_{20}H_{39}O_2H$ (Table 6) show that the C form is monoclinic ($P2_1/a$, $Z = 4$). The differences compared to the previous single crystal results (ref. 25) can be explained in terms of the thermal expansion of the cell. According to these results, the cell volume of $C_{10}H_{19}O_2H$ changes from 1063 Å^3 at 170 K to 1116 Å^3 at 270 K. Consequently, a volume of 1129 Å^3 is expected at room temperature.

A linear evolution of $c\sin\beta$ (the thickness of a double layer of molecules) along the different members of the family is observed for the C form, whereas a and b parameters can be considered constant, concluding that the C form is isostructural for the compounds studied.

The monoclinic B_m and E_m polytypes of $C_{16}H_{31}O_2H$, $C_{18}H_{35}O_2H$ and $C_{20}H_{39}O_2H$ have space group $P2_1/a$ with $Z = 4$, while the orthorhombic B_o and E_o polytypes have *Pbca* space group with $Z = 8$. Cell parameters are reported in Tables 7 and 8.

According to the variation of the unit cell parameters, the B_o form is isostructural for acids $C_{18}H_{35}O_2H$ and $C_{20}H_{39}O_2H$ and the B_m and E_m forms are isostructural for acids $C_{16}H_{31}O_2H$, $C_{18}H_{35}O_2H$ and $C_{20}H_{39}O_2H$.

The cell parameters of the triclinic forms need further crystallographic investigation in order to be determined. To date, the powder X-ray diffraction patterns, the SEM images and the DSC analysis confirm the existence of two different types of triclinic forms: one that matches the characteristics reported by Kobayashi *et al.*[30] for the A_2 form of $C_{16}H_{31}O_2H$, and the other that matches the characteristics reported by von Sydow[29] and Goto and Asada[14] for the A_{super} form of $C_{12}H_{23}O_2H$. For that reason we keep the notation. The

Table 7 Cell parameters for the orthorhombic polytype (*Pbca*, $Z = 8$) of the B form

Phase	Acid	a/Å	b/Å	c/Å	V/Å^3	Ref.
B_o	$C_{18}H_{35}O_2H$	7.408(3)	5.587(3)	87.69(6)	3629.4	This work
	$C_{18}H_{35}O_2H$	7.404(1)	5.591(1)	87.662(9)	3628.7	22
	$C_{20}H_{39}O_2H$	7.412(1)	5.592(2)	96.73(2)	4009.3	This work

Table 6 Cell parameters of the C form ($P2_1/a$, $Z = 4$)

Acid	a/Å	b/Å	c/Å	β/°	V/Å^3	T/K	Ref.
$C_{10}H_{19}O_2H$	9.834(1)	4.940(1)	37.47(1)	141.94(1)	1122.2	298	This work
$C_{10}H_{19}O_2H$	9.3977(6)	4.9612(3)	37.372(2)	142.405(4)	1063.0	170	25[a]
$C_{10}H_{19}O_2H$	9.716(7)	4.973(5)	37.59(3)	142.10(8)	1115.7	270	25[a]
$C_{12}H_{23}O_2H$	9.604(1)	4.953(1)	42.30(1)	139.78(1)	1299.5	298	This work
$C_{12}H_{23}O_2H$	9.5266(6)	4.9627(3)	42.379(2)	139.905(2)	1290.4	270	25[a]
$C_{12}H_{23}O_2H$	9.52(2)	4.97(1)	35.39(7)	129.22(2)	1297.2	—	49
$C_{12}H_{23}O_2H$	9.63(2)	4.966(4)	35.58(8)	129.6(1)	1311.0	—	50
$C_{14}H_{27}O_2H$	9.497(1)	4.972(1)	44.45(1)	134.81(1)	1489.0	298	This work
$C_{14}H_{27}O_2H$	9.4260(11)	4.9652(5)	43.972(3)	134.311(4)	1472.6	270	25[a]
$C_{14}H_{27}O_2H$	9.51(2)	4.968(4)	40.71(8)	129.1(1)	1492.6	—	50
$C_{16}H_{31}O_2H$	9.440(1)	4.975(1)	45.74(1)	128.65(1)	1677.5	298	This work
$C_{16}H_{31}O_2H$	9.406(3)	4.949(2)	45.61(1)	128.661(5)	1658.0	298	26[a]
$C_{18}H_{35}O_2H$	9.354(1)	4.960(1)	50.82(1)	128.38(1)	1848.3	298	This work
$C_{18}H_{35}O_2H$	9.36(2)	4.95(1)	50.7(1)	128.3(3)	1843.5	—	27
$C_{18}H_{35}O_2H$	9.36(2)	4.956(4)	50.76(8)	128.2(1)	1850.4	—	50
$C_{20}H_{39}O_2H$	9.318(1)	4.956(1)	53.73(1)	124.98(1)	2033.2	298	This work

[a] Structures originally reported in the conventional space group $P21/c$ and transformed to $P2_1/a$.

Table 8 Cell parameters for the monoclinic polytype ($P2_1/a$, $Z = 4$) of the B and E forms

Phase	Acid	a/Å	b/Å	c/Å	β/°	V/Å^3	Ref.
E_m	$C_{16}H_{31}O_2H$	5.622(1)	7.379(1)	45.67(1)	119.64(1)	1646.5	This work
	$C_{18}H_{35}O_2H$	5.608(1)	7.386(1)	50.75(1)	119.44(1)	1830.7	This work
	$C_{18}H_{35}O_2H$	5.603(1)	7.360(1)	50.789(9)	119.40(2)	1824.6	23
	$C_{20}H_{39}O_2H$	5.601(1)	7.384(1)	54.05(1)	115.34(1)	2020.1	This work
B_m	$C_{16}H_{31}O_2H$	5.592(1)	7.415(1)	46.30(1)	121.80(1)	1631.5	This work
	$C_{18}H_{35}O_2H$	5.598(1)	7.397(1)	49.44(2)	117.24(1)	1820.3	This work
	$C_{18}H_{35}O_2H$	5.587(10)	7.386(6)	49.33(8)	117.24(9)	1809.9	21
	$C_{20}H_{39}O_2H$	5.582(1)	7.404(1)	54.57(1)	117.60(1)	1998.7	This work

differences observed between the two triclinic forms are explained in the following sections.

X-Ray powder diffraction and differential scanning calorimetry (DSC)

To identify the different crystal forms it is convenient to divide the experimental powder diffraction pattern into two regions, the low angle region (3–15° in 2θ) and the middle angle region (19–25° in 2θ).

In the low angle region (Fig. 5), the position of the (0 0 l) reflections for the $P2_1/a$ space group and the *Pbca* space group allows the unambiguous identification of the C and the A_2 forms (Fig. 5a). The presence of the $E_{o/m}$ or the $B_{o/m}$ forms, or even a mixture of them, can be detected according to this family of reflections but they cannot be distinguished due to their similar structures (Fig. 5c). The pattern of the A_{super} form (Fig. 5b) shows the evenly spaced (0 0 l) reflections, with l odd absent, typical for *n*-carboxylic acids, plus further reflections that correspond to the (0 k l), and the (0 k $\bar{l}$) family, the rest of the pattern being similar to that of the A_2 form.

To distinguish between the B and the E forms and their orthorhombic and monoclinic polytypes, we propose guidelines 1 and 2, respectively:

(1) As shown in Fig. 6a for the E_o and B_o forms of $C_{18}H_{35}O_2H$, the (2 0 0) reflection (at a 2θ value around 24.1° within the reported experimental conditions) is shifted to high angles for the E form, while it is shifted to low angles for the B form, independently of the polytype considered.

(2) As shown in Fig. 6b for the B_o and the B_m polytypes of $C_{18}H_{35}O_2H$, the orthorhombic polytype has three reflections more than the monoclinic polytype. As observed from Fig. 6b, all reflections for the B_m and B_o polytypes of $C_{18}H_{35}O_2H$ overlap except the three reflections of the B_o form that correspond to (1 1 5), (1 1 7) and (1 1 11) (at a 2θ value of 20.52°, 21.12° and 22.82°, respectively, within the reported experimental conditions). An analogous behaviour is shown by the E_m and E_o polytypes, where all reflections overlap for both polytypes, except the reflections (1 1 6), (1 1 8), (1 1 10) and (1 1 12) of the orthorhombic polytype (at a 2θ value of 20.78°, 21.46°, 22.30°, 23.29°, respectively, within the already-mentioned experimental conditions).

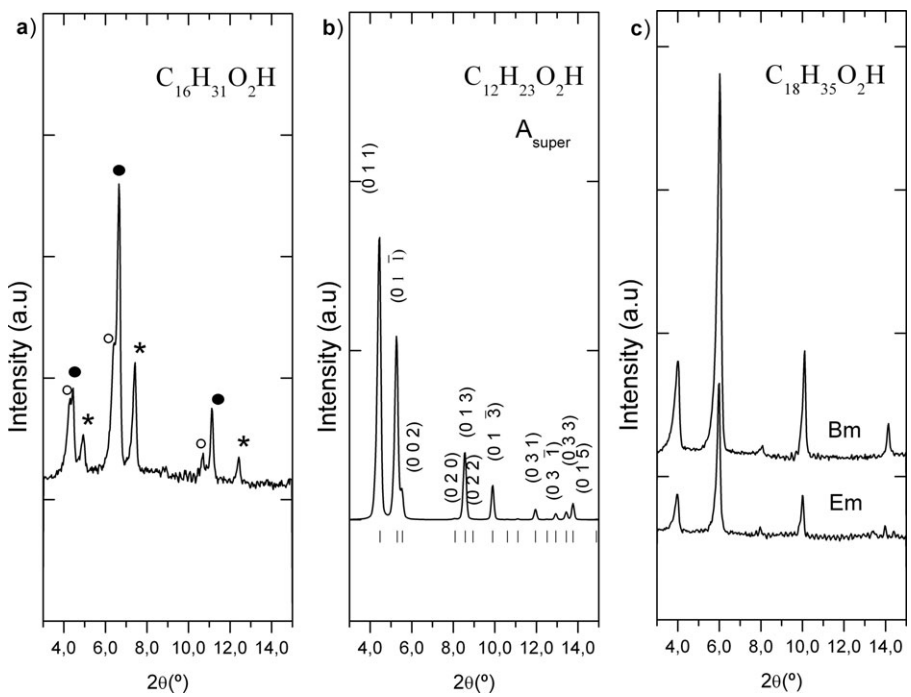

Fig. 5 Low angle X-ray powder diffraction patterns of (a) a mixture of A_2 (○), E_m (●) and C (*) forms of $C_{16}H_{31}O_2H$, (b) A_{super} form of $C_{12}H_{23}O_2H$ simulated from single crystal data[14] and (c) B_m and E_m forms of $C_{18}H_{35}O_2H$.

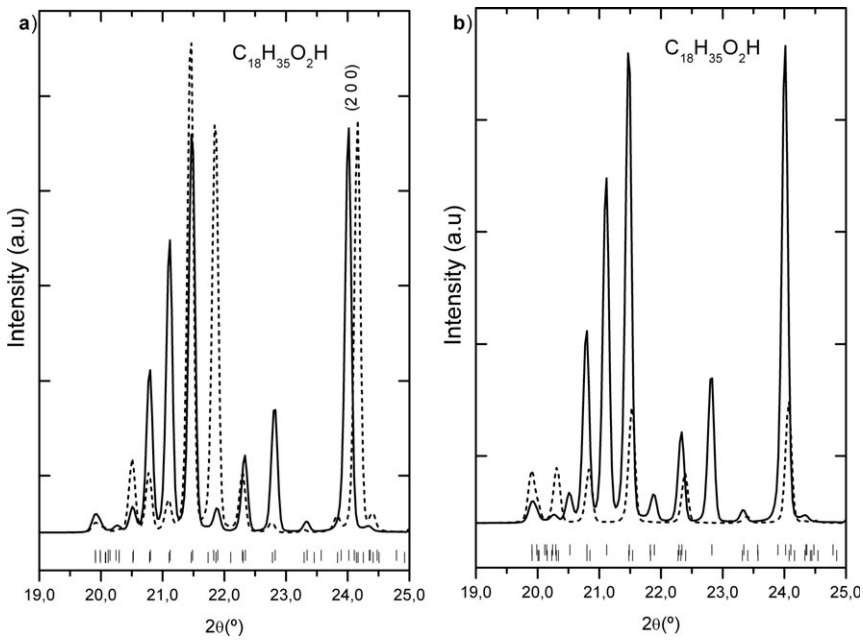

Fig. 6 Middle angle X-ray powder diffraction patterns and Bragg positions from single crystal data[21,22,24] of (a) the form B_o (—) and the form E_o (--) of $C_{18}H_{35}O_2H$ and of (b) the B_m (--) and the B_o (—) forms and of $C_{18}H_{35}O_2H$.

When traces of one form are present in a sample, DSC is a suitable technique to confirm it since it has higher sensitivity than powder X-ray diffraction.

Temperature, shape and enthalpy of the phase transitions are an indicator of the form present (Fig. 7). The $A_{super} \rightarrow C$ transformation has the highest transition point, occurs just before the melting and the curve is overlapped by the melting peak (Fig. 7a). The $A_2 \rightarrow C$ transition has a broad peak and occurs at a higher temperature than $B_{o/m} \rightarrow C$ and $E_{o/m} \rightarrow C$ (Fig. 4a). The transitions from $B_{o/m}$ and from $E_{o/m}$ modifications to the C form take place in the same range of temperatures. Still, a significantly more energetic and sharper peak is characteristic for the $B_{o/m} \rightarrow C$ transformation than for the $E_{o/m} \rightarrow C$ one; for the latter, a broad peak is observed (Fig. 7b). The coincidence in temperature but not in energy among the $B_{o/m}$ and $E_{o/m}$ to C transitions can be explained in terms of their structures, since the transformation $B_{o/m} \rightarrow C$ involves a change in the molecular conformation of the C_2–C_3 bond from *gauche* to all-*trans*, which it is expected to need more energy than the transition from $E_{o/m}$ to C.

To conclude, X-ray powder diffraction allows the identification of the C and the triclinic forms (A_{super} and A_2). However, the identification of the B and E forms is not so straightforward, even more when mixtures of forms are present—which is the most common case. In such cases, DSC analyses and infrared spectroscopy, as explained in the next subsection, are the way forward to distinguish between the E and the B forms.

Infrared spectroscopy (FT-IR)

The infrared spectra of the carboxylic acids show the characteristic bands of the *n*-alkanes[51] plus the bands caused by the vibrations of the carboxyl group (Table 9) and its interaction with the hydrocarbon chain. The vibration mode assignment is based on previous studies.[28,30,52,53]

By means of infrared spectroscopy with polycrystalline samples, the forms A and B can be identified and distinguished from E or C, since there are characteristic bands associated with their specific molecular conformation. The different polytypes or triclinic modifications are only distinguishable by single crystal polarized infrared spectroscopy. Thus, the distinction between the polytypes and the modifications of the A form is disregarded in this section. Representative FT-IR spectra of the A_2, E_m, C and B_o forms are shown in Fig. 8.

The ν(C=O) band (1721 and 1698 cm^{-1}) is split only for the B form due to the chain tilt of the molecules within the unit cell that, together with the *gauche* conformation of the molecules, allows the carboxyl groups in neighbouring dimers to be close enough to interact. The $\delta(CH_2)$ (1472 cm^{-1}) and the $r(CH_2)$ (718 cm^{-1}) bands are single bands for the A form, otherwise, the bands are split due to a different chain–chain interaction of the molecules in the subcell. An exhaustive description of the different forms in terms of the subcell is found in ref. 54. For the matter of concern, the different triclinic A forms have a triclinic subcell, T||, with parallel molecules. Instead, the E, B and C forms have an orthorhombic subcell, O⊥, with perpendicular molecules. Therefore, the different type of interaction between the chains induces the splitting of the bands associated with the methylene group.

The $\omega(CH_2)$ progression of bands (1320–1180 cm^{-1}) coupled with the carboxyl vibrations appears as a regularly spaced succession of bands for the structures with all-*trans* molecules (E and C). The *gauche* conformation of the molecules in the B form and the particular conformation of the molecules in the A forms cause strong interactions between the methylene and the carboxyl group, making the progression rather irregular.

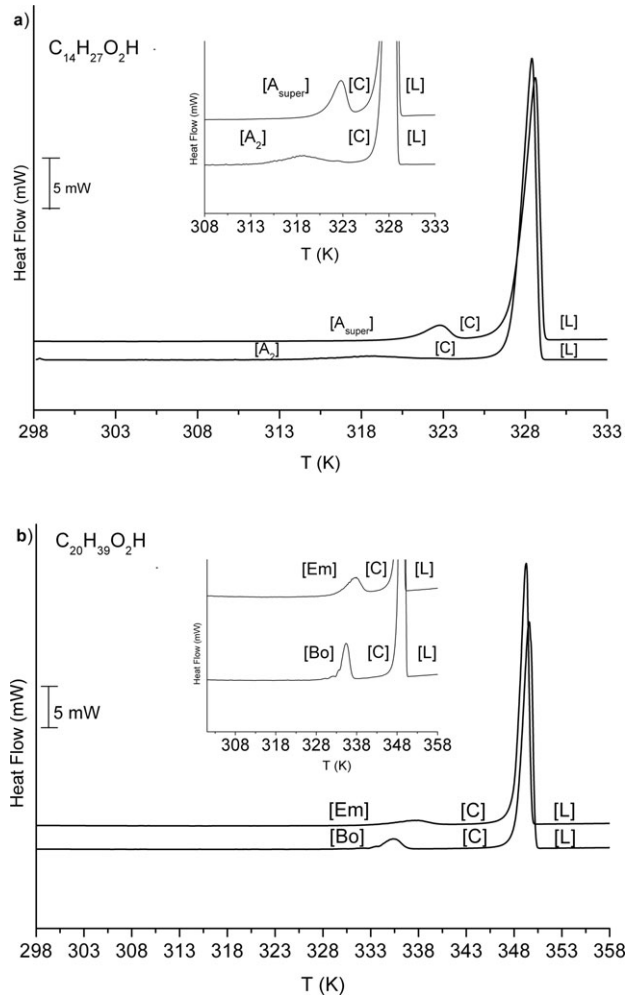

Fig. 7 DSC curves of (a) A_2 and A_{super} forms of $C_{14}H_{27}O_2H$ and (b) E_m and B_o forms of $C_{20}H_{39}O_2H$ recorded at 2 K min^{-1}. Insets: expansions of the DSC curves close to the transition temperature.

The *gauche* conformation of molecules of the B form also affects the ν(C–C) vibrations (1150–1000 cm^{-1}). The band at 1122 cm^{-1} is associated to the C–C stretching coupled with the carboxyl group whereas the band at 1098 cm^{-1} is associated to the coupling with the methyl terminal group showing for the B form a band at 1122 cm^{-1} significantly more intense than the one at 1098 cm^{-1}. The relative intensities are inverted for the

Table 9 Most frequent vibrations of the carboxylic functional group as dimer

Type of vibration	Frequency/ cm^{-1}	Intensity
OH stretching	≈3000	Broad and strong
Overtone and combination bands	2700–2500	Medium–weak
C═O stretching asymmetric	1740–1660	Broad and very strong
C═O stretching symmetric	1687–1625	Weak
C–OH bending in plane	1440–1395	Medium
C–O stretching	1315–1280	Strong
O–H bending out of plane	960–875	Medium
O–C═O	690–630	Strong

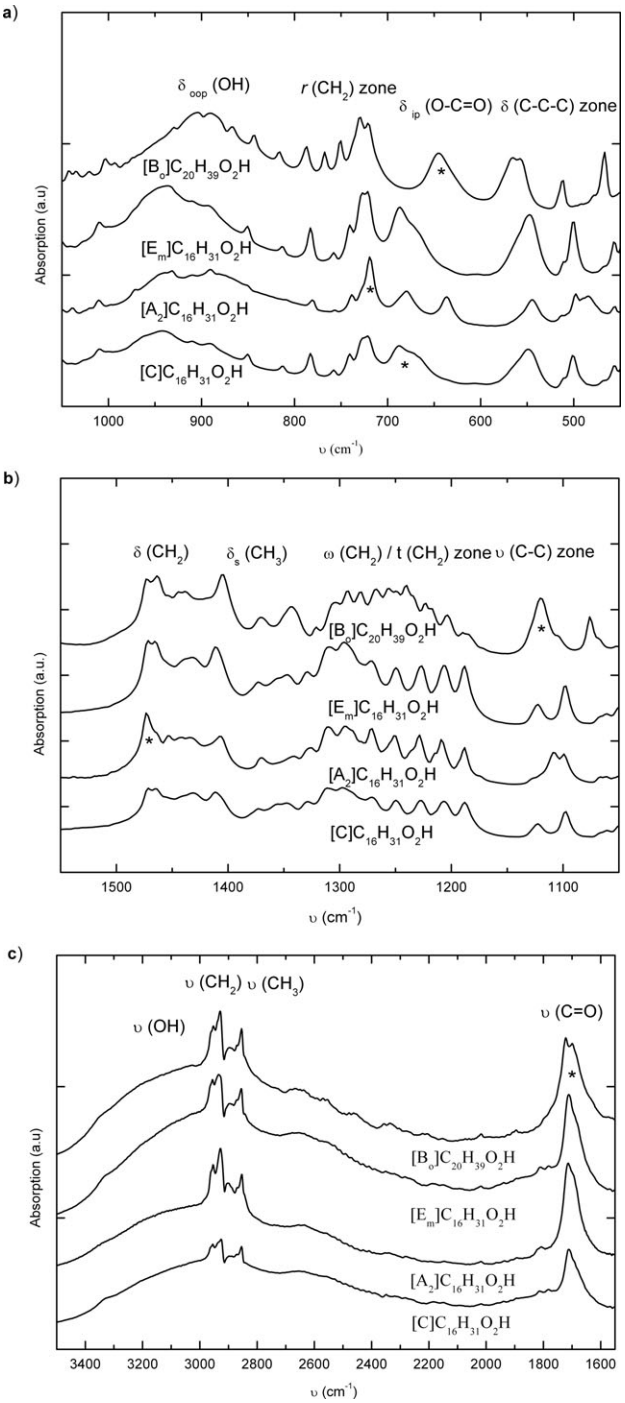

Fig. 8 Main zones of the infrared spectra at 298 K of $C_{16}H_{31}O_2H$ in A_2, E_m and C forms and of $C_{20}H_{39}O_2H$ in B_o form. Asterisks indicate the most relevant bands to identify polymorphs.

E, C and A forms. The unique band to distinguish the E and C forms is at the δ_{oop}(OH) zone (960–875 cm^{-1}), which is highly sensitive to the conformation of the polymethylene skeletal chain; broad single bands are found at 937 cm^{-1} and 941 cm^{-1} for the E and C forms, respectively. The δ_{ip}(O–C═O) band is an intense single band at 645 cm^{-1} for the B form. The band is shifted to 686 cm^{-1} for the E form. A double band is observed for the triclinic forms at 683 and 638 cm^{-1}, in agreement with

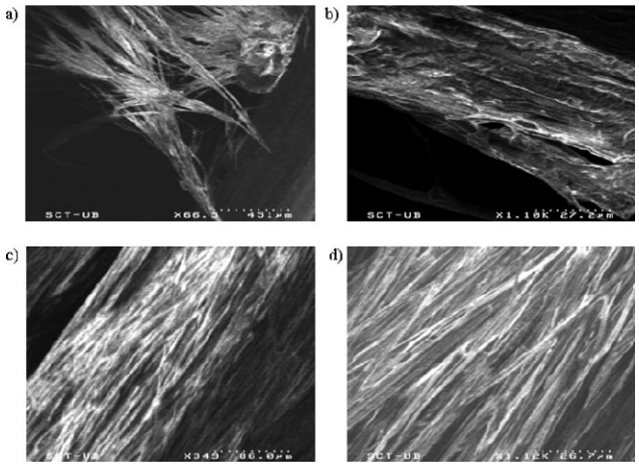

Fig. 9 SEM images of (a, b) A_2 and (c, d) A_{super} forms of $C_{14}H_{27}O_2H$.

the two different molecular conformations in the triclinic structures. A broad double band at 688 and 668 cm^{-1} is assigned to a *cis*/*trans* tautomeric equilibrium exclusive of the C form that involves the transfer of a proton between the molecules of the dimer unit.[55] The tautomeric equilibrium is only possible for the C form because of its suitable oxygen–oxygen distances of 2.62 Å. The proton transfer has not been observed in the other forms due to larger oxygen–oxygen distances.[21–24]

To summarize, FT-IR spectroscopy is the proper technique to distinguish among the E and B forms and therefore it complements the information extracted from X-ray powder diffraction data. It is also possible to identify the triclinic forms by means of this technique as has been explained.

Scanning electron microscopy (SEM)

Crystals of the A_2 form have needle-like shape and dendritic growth (Fig. 9a). In a similar way, the A_{super} form crystallizes as long fibres (Fig. 9c). Images taken with greater magnification show that the needle-like crystals of the A_2 form (Fig. 9b) have an irregular surface rather than the fibrous aspect of the A_{super} form (Fig. 9d), confirming the existence of two different types of triclinic structures as observed by powder X-ray diffraction and DSC experiments.

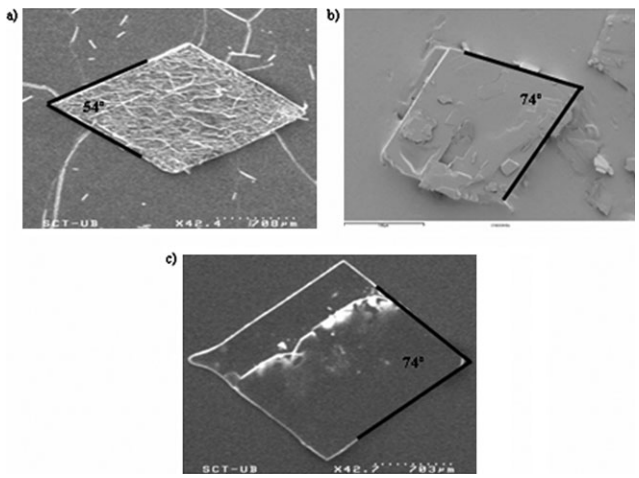

Fig. 10 SEM images of (a) a crystal of the C form of $C_{16}H_{31}O_2H$, (b) a crystal of the E form of $C_{16}H_{31}O_2H$, (c) a crystal of the B form of $C_{18}H_{35}O_2H$.

Fig. 10a shows the plate-like crystals with prismatic shape and an acute angle of around 54°, characteristic of the C form. Similar crystals with a larger acute angle (around 74°) are characteristic of the $E_{o/m}$ (Fig. 10b) and the $B_{o/m}$ forms (Fig. 10c). The structural similarities observed by X-ray powder diffraction analysis among the B and E forms agree with their identical morphology.

The C, $B_{o/m}$, and $E_{o/m}$ forms, with plate-like morphology, have the carboxyl groups and methyl groups in different terminal planes parallel to the *ab* plane. This plane corresponds to the faces with the lowest attachment energy, which developed slower and therefore have the most morphological importance. In the A_{super} form, each terminal plane contains both carboxyl and methyl terminal groups, which will cause strong hydrogen bond interactions along a direction rather than in a plane, giving rise to long fibres.

Moreover, when a mixture of forms was determined according to X-ray powder diffraction and DSC measurements, the individual morphologies were identified by SEM.

Conclusions

The DSC analyses on even saturated carboxylic acids reveal high enthalpies for the solid–solid transition and especially for the solid–liquid process. That makes saturated *n*-carboxylic acids and their alloys suitable candidates as molecular alloy phase change materials (MAPCM) to be used in the fields of energy storage and thermal protection.

The polymorphism of this family of compounds depends on the solvent used for crystallization, the temperature and the rate of crystallization, the purity and the parity of the acid. Triclinic forms predominate for acids with up to 14 carbon atoms, while monoclinic and orthorhombic forms (B, E and C) predominate for longer members of the family, in the range studied. Whatever the forms present at room temperature all of them transform irreversibly to the C form before melting, which is the stable form at high temperatures, the B form being the stable one at room temperature.

According to X-ray powder diffraction, the forms C ($P2_1/a$, $Z = 4$), B_o ($Pbca$, $Z = 8$), B_m ($P2_1/a$, $Z = 4$) and E_m ($P2_1/a$, $Z = 4$) are isostructural for the compounds studied herein, but the C, B_o, B_m, and E_m forms are not isostructural to each other.

The family of the (0 0 *l*) reflections in the diffraction pattern is used to identify the A_2, the A_{super} and the C forms. The A_{super} form gives further (0 *k l*) and (0 *k* $\bar{l}$) reflections in this region. On the other hand, the middle angle region of the pattern provides the necessary information to distinguish among B and E forms and among their monoclinic and orthorhombic polytypes, as discussed in the text.

The infrared spectra recorded on polycrystalline samples show the characteristic bands due to molecules with a *gauche* conformation involving the C_2–C_3 bond characteristic for B_o and B_m forms as well as the intermediate conformation of the

C_1–C_2 bond of the triclinic forms. It is the most suitable technique to differentiate between the $B_{o/m}$ and $E_{o/m}$ forms.

SEM images confirm the high structural similarity between the $B_{o/m}$ and $E_{o/m}$ forms since both show exactly the same plate-like crystals, while needle-like crystals are observed for the A_2 form and fibres for the A_{super} form.

Acknowledgements

We thank Dr Maria Barrio for her collaboration and scientific advice in the realization of the high pressure DSC measurements and Silvia Miramunt for the experimental measurements. We also thank the Ministerio de Ciencia y Tecnología for the financial support through the CICYT (grant: BES-2002-1855, project number: MAT2001-3352), the Generalitat de Catalunya through the Grup Consolidat (1996SGR0039), Xarxa Temàtica Aliatges Moleculars (20031XT-00077) and Centre de Referència en Materials Avançats per l'Energia (CeRMAE).

References

1 D. Mondieig, F. Rajabalee, V. Métivaud, H. A. J. Oonk and M. A. Cuevas-Diarte, *Chem. Mater*., 2004, **16**, 786.
2 V. Métivaud, V. A. Lefèvre, L. Ventolà, P. Négrier, E. Moreno, T. Calvet, D. Mondieig and M. A. Cuevas-Diarte, *Chem. Mater*., 2005, **17**, 3302.
3 L. Ventolà, M. Ramírez, T. Calvet, X. Solans, M. A. Cuevas-Diarte, P. Negrier, D. Mondieig, J. C. van Miltenburg and H. A. J. Oonk, *Chem. Mater*., 2002, **14**, 508.
4 L. Ventolà, T. Calvet, M. A. Cuevas-Diarte, H. A. J. Oonk and D. Mondieig, *Phys. Chem. Chem. Phys*., 2004, **6**, 3726.
5 L. Ventolà, T. Calvet, M. A. Cuevas-Diarte, V. Métivaud, D. Mondieig and H. A. J. Oonk, *Mater. Res. Innovatations*, 2002, **6**, 284.
6 D. Mondieig, F. Rajabalee, A. Laprie, H. A. J. Oonk, T. Calvet and M. A. Cuevas-Diarte, *Transfus. Apher. Sci*., 2003, **28**, 143.
7 V. Métivaud, L. Ventolà, M. A. Cuevas-Diarte, T. Calvet, D. Mondieig, *IEA, ECES IA, Annex 17*, 6th workshop, Arvika, Sweden, 8–9 June, 2004.
8 E. von Sydow, *Ark. Kemi*., 1956, **9**, 231.
9 K. Sato and M. Kobayashi, *Crystals 13*, Springer-Verlag, Berlin, 1991.
10 M. Goto, *Yukagaku*, 1987, **36**, 909.
11 G. Gbabode, P. Négrier, D. Mondieig, E. Moreno, T. Calvet and M. A. Cuevas-Diarte, *Chem.–Eur. J*., 2007, **13**, 3150.
12 J. Bernstein, R. E. Davis, L. Shimoi and N. L. Chang, *Angew. Chem., Int. Ed. Engl*., 1995, **34**, 1555.
13 T. R. Lomer, *Acta Crystallogr*., 1963, **16**, 984.
14 M. Goto and E. Asada, *Bull. Chem. Soc. Jpn*., 1978, **51**(1), 70.
15 M. Goto and E. Asada, *Bull. Chem. Soc. Jpn*., 1980, **53**(8), 2111.
16 E. von Sydow, *Acta Crystallogr*., 1954, **7**, 529.
17 E. von Sydow, *Acta Crystallogr*., 1955, **8**, 845.
18 (*a*) E. von Sydow, *Acta Crystallogr*., 1954, **7**, 823; (*b*) E. von Sydow, *Acta Crystallogr*., 1955, **8**, 846.
19 M. Goto and E. Asada, *Bull. Chem. Soc. Jpn*., 1984, **57**(4), 1145.
20 G. Gbabode, P. Négrier, D. Mondieig, J. M. Leger, E. Moreno, T. Calvet and M. A. Cuevas-Diarte, *Anal. Sci*., 2006, **22**(11), 269.
21 M. Goto and E. Asada, *Bull. Chem. Soc. Jpn*., 1978, **51**(9), 2456.
22 F. Kaneko, H. Sakashita and M. Kobayshi, *Acta Crystallogr., Sect. C: Cryst. Struct. Commun*., 1994, **C50**, 245.
23 F. Kaneko, M. Kobayashi, Y. Kitagawa and Y. Matsuura, *Acta Crystallogr., Sect. C: Cryst. Struct. Commun*., 1990, **C46**, 1490.
24 F. Kaneko, H. Sakashita and M. Kobayshi, *Acta Crystallogr., Sect. C: Cryst. Struct. Commun*., 1994, **C50**, 247.
25 A. D. Bond, *New J. Chem*., 2004, **28**(1), 104.
26 E. Moreno, R. Cordobilla, T. Calvet, M. A. Cuevas-Diarte, F. J. Lahoz and A. I. Balana, *Acta Crystallogr., Sect. C: Cryst. Struct. Commun*., 2006, **C62**, 131.
27 V. Malta, G. Celotti, R. Zannetti and A. F. Martelli, *J. Chem. Soc. B*, 1971, 548.
28 R. F. Holland and R. Nielsen, *Acta Crystallogr*., 1963, **16**, 984.
29 E. von Sydow, *Acta Chem. Scand. (1947–1973)*, 1956, **10**, 1.
30 T. Kobayashi, M. Kobayashi and H. Tadokoro, *Mol. Cryst. Liq. Cryst*., 1984, **104**, 193.
31 O. Masson and A. Ramponi, *PEAKOC Program*, Laboratoire de Matériaux Céramiques et Traitements de Surfaces, CNRS-ENSCI, Limoges, France, 1996.
32 M. A. Neumann, *J. Appl. Crystallogr*., 2003, **36**, 356.
33 MS Modeling (Materials Studio) 3.0 http://www.accelrys.com/mstudio/ms_modeling/.
34 G. E. Engel, S. Wilke, K. D. M. Harrys and F. J. J. Leusen, *J. Appl. Crystallogr*., 1999, **32**, 1169.
35 A. Boultif and D. Louer, *J. Appl. Crystallogr*., 1991, **24**, 987.
36 J. Rodriguez-Carvajal, *FULLPROF Program*, Laboratoire leon Brillouin, Paris, France, 1998.
37 N. Pingel, U. Poser and A. Würflinger, *J. Chem. Soc., Faraday Trans. 1*, 1984, **80**, 3221.
38 G. L. Clark, *Applied X-Ray*, McGraw-Hill, New York, 1955.
39 E. Stenhagen and E. von Sydow, *Ark. Kemi*., 1952, **6**(29), 309.
40 R. C. F. Schaake, J. C. van Miltenburg and C. G. de Kruif, *J. Chem. Thermodyn*., 1982, **14**, 771.
41 N. Adriaansen, H. Dekker and J. Coops, *Recl. Trav. Chim. Pays-Bas*, 1964, **83**(6), 557.
42 W. Beckman, R. Boistelle and K. Sato, *J. Chem. Eng. Data*, 1984, **29**, 211.
43 K. Sato, K. Suzuki, M. Okada and N. Garti, *J. Cryst. Growth*, 1985, **72**, 699.
44 K. Sato and R. Boistelle, *J. Cryst. Growth*, 1984, **66**, 441.
45 K. Sato and R. Boistelle, *J. Colloid Interface Sci*., 1983, **94**, 593.
46 A. Würflinger and G. M. Schneider, *Ber. Bunsen-Ges. Phys. Chem*., 1973, **77**, 121.
47 H. Sun, *J. Phys. Chem. B*, 1998, **102**, 7338.
48 A. Gavezzotti and G. Filippini, *Theoretical Aspects and Computer modeling*, J. Wiley and Sons, Chichester, 1997, ch. 3, pp. 61–97.
49 V. Vand, W. M. Morley and T. R. Lomer, *Acta Crystallogr*., 1951, **4**, 324.
50 S. Abrahamsson and E. von Sydow, *Acta Crystallogr*., 1954, **7**, 591.
51 (*a*) J. H. Schachtschneider and R. G. Snyder, *Spectrochim. Acta*, 1963, **19**, 85; (*b*) J. H. Schachtschneider and R. G. Snyder, *Spectrochim. Acta*, 1963, **19**, 117.
52 R. F. Holland and J. Nielsen, *J. Mol. Spectrosc*., 1962, **9**, 436.
53 F. Kaneko, K. Tashiro and M. Kobayashi, *J. Cryst. Growth*, 1999, **198**, 1352.
54 N. Garti and K. Sato, *Crystallization and polymorphism of fats and fatty acids*, Marcel Dekker Inc., New York, 1988.
55 S. Hayashi and J. Umemura, *J. Chem. Phys*., 1975, **63**, 1732.